Vol 12 No 9, September 2003
1009-1963/2003/12(09)/1026-07

Chinese Physics

© 2003 Chin. Phys. Soc.
and IOP Publishing Ltd

# Study of far-infrared reflection and Raman scattering spectra in reactive ion, etched ZnTe*

Wu Sen(吴 森)[a], Shen Wen-Zhong(沈文忠)[a]†,
Ogawa Hiroshi(小川博司)[b], and Guo Qi-Xin(郭其新)[b]

[a] *Department of Physics, Shanghai Jiao Tong University, Shanghai* 200030, *China*
[b] *Department of Electrical and Electronic Engineering, Faculty of Science and Engineering, Saga University, Saga* 840-8502, *Japan*

(Received 22 April 2003)

Far-infrared reflection and Raman scattering measurements have been carried out on reactive ion, etched p-ZnTe samples. The averaged thickness of the surface damaged layer is found to be in the range of 1.0–1.5$\mu$m, and the, etch-induced defect density is in the order of $10^{18}$cm$^{-3}$. The Raman intensity ratio between the second-order Raman peaks and the first-order longitudinal optical phonons reveals an increase trend with the radio frequency (rf) power. With the aid of related theories, we discuss the effects of the rf plasma power and the concentration of $CH_4/H_2$ on the damage, disorder, and the second-order Raman structures in p-ZnTe samples.

**Keywords:** reactive ion, etched, spectroscopic measurements, ZnTe
**PACC:** 7830G, 7830L, 7155F

## 1. Introduction

With the rapid progress in the micromation and integration of the semiconductor optoelectronic device industry, advanced patterning technology is required to be developed. In comparison with the traditional wet, etching, the reactive ion, etching (RIE), a dry, etching process which combines the selectivity of chemical processes and the directionality of physical processes, has become an effective technique for microfabrication and pattern transfer in semiconductor optoelectronics due to its easily controlled characteristics and its ability to produce an anisotropic microsized structure. RIE has been generally considered as the main developing direction of, etching. It has been reported that the RIE technology could be influenced by many factors, such as the concentration and flux of, etching gases, the rf plasma power, the material selectivity of the gases, the plasma pressure and so on.[1] Since RIE is a mixed effect of physical bombardment and chemical, etching, it is very interesting to study the damage effects. Different information has been provided in the damaged layers produced under different, etching conditions. Through the study of the damaged layers, we can obtain qualitatively or quantitatively the effects of, etching conditions on the novel properties in the, etched materials, which provide the theoretical and experimental basis for the material growth and device fabrication. In the selection of, etching gases, the methane and hydrogen ($CH_4/H_2$), which are relatively easy to handle, less toxic and corrosive than chloride and bromide gases, have been widely employed recently.[2,3]

The previous RIE studies mainly concentrate on the GaAs crystals. To evaluate the damage of the RIE technology on the crystal surface and lattice, various techniques, such as x-ray photoelectron spectroscopy (XPS),[4,5] Schottky diode performance,[6] photoconductivity measurement,[3,7] and photoluminescence (PL),[8,9] have been employed. Zinc telluride (ZnTe), a typical II-VI semiconductor with a cubic zinc-blende structure, is an important optoelectronic material[10−12] and has a wide applications in the green laser diodes, optical waveguides, optical modulators, etc. In order to study the effects of dry, etching on the optical and electrical properties of ZnTe

*Project supported by the National Natural Science Foundation of China (Grant No 10125416).
†Corresponding author. E-mail: wzshen@sjtu.edu.cn

for high-quality ZnTe optoelectronic devices, the RIE technology has been employed on this important semiconductor in recent years.[2,13]

Compared with XPS and other methods, far-infrared (FIR) reflection and Raman scattering are not only as contactless and nondestructive, but also as effective methods to study the lattice vibration, lattice structure, and the influence on electronic performance.[14–17] Wang *et al*[16] and Roughani *et al*[17] have used the coupled longitudinal-optical (LO) phonon-plasmon (LPP) mode to evaluate the damage of RIE in $n^+$-GaAs. Nevertheless, to the best of our knowledge, there are no studies of FIR reflection and Raman scattering characteristics in RIE ZnTe so far. In this paper, we report on the detailed investigation of the FIR reflection and Raman scattering spectra in $CH_4/H_2$, etched ZnTe crystals. By fitting the FIR reflection spectra with a classical oscillator model, we obtain the average thickness and defect density of the surface damaged layer, together with the effects of rf plasma powers and gas concentration on the, etching performance. The Raman scattering spectra have been discussed to reveal the effects of, etching conditions on the lattice disorder and the intensity of the second-order Raman modes.

## 2. Experiments

The p-type ZnTe crystals studied with a carrier concentration of $10^{16}$–$3\times10^{17}$cm$^{-3}$ were prepared in a Bridgman furnace heated to 1200°C. The ZnTe samples with a (100)-oriented surface were mechanically polished with 0.05$\mu$m alundum. The samples were degreased in organic solvents and then, etched in Br methanol for 40s, followed by a methanol rinse. In order to evaluate the quality of these ZnTe samples, x-ray diffraction (XRD) measurements were carried out on a Shimadzu XD-3A system with Cu$K\alpha$ radiation ($\lambda_x$=0.15405nm). Figure 1 shows the XRD results for the unetched (as-grown) ZnTe sample (No.1). Two strong diffraction peaks appear at $2\theta$=29.08° and 60.12° with a full-width at half-maximum of 0.23° and 0.22°, respectively, indicating the high quality of the ZnTe samples. According to the equation $2L_{\rm d}\sin\theta = n\lambda_x$, we can obtain the lattice spacing $L_{\rm d}$ when $n$=1, based on which we can conclude that these two diffraction peaks correspond to the (200) and (400) lattice planes of the cubic ZnTe. The disappearance of the (100) diffraction peak is due to the extinction effect of the surface.

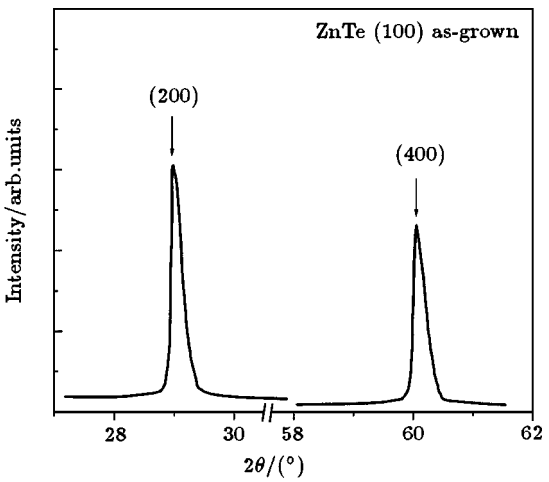



**Fig.1.** XRD results of the unetched (as-grown) ZnTe sample (No.1). The peaks at 29.08° and 60.12° with a full width at half maximum of 0.23° and 0.22° correspond to (200) and (400)-planes of the cubic ZnTe, respectively.

Five similar ZnTe crystals have been, etched for 10min under different rf plasma powers and $CH_4/H_2$ concentrations and marked as sample Nos.2–6. The RIE experiments were carried out in a load-locked SAMCO RIE-200L system with the plasma pressure of 25Pa and the detailed, etching conditions are listed in Table 1. The FIR reflection measurements on these RIE ZnTe crystals were performed at room temperature on a Nicolet Nexus 870 Fourier transform infrared (FTIR) spectrometer with a DTGS polyethylene detector, solid substrate beamsplitter for the range of 50–700cm$^{-1}$ under the near-normal incidence geometry (less than 10° incidence angle). The Raman scattering measurements were also performed on the Nicolet Nexus 870 FTIR Raman accessory module with a $CaF_2$ beamsplitter and a liquid-nitrogen-cooled Ge detector. The samples were excited by a 1064nm (9398cm$^{-1}$) laser line with a backscattering geometry. The resolutions of the FIR reflection and Raman measurements are 4.0 and 1.0cm$^{-1}$, respectively.

**Table 1.** Parameters of multiple oscillators for the fitting calculations of measured FIR reflection spectra in RIE ZnTe crystals, together with the dry, etching conditions. The as-grown parameters have been adopted for the undamaged ZnTe crystals in the five, etched ZnTe crystals.

| Sample No. | $CH_4$/sccm | $H_2$/sccm | $CH_4$ concen./% | rf power/W | $d/\mu$m | $\omega_{TO}/cm^{-1}$ | $S$ | $\gamma/cm^{-1}$ |
|---|---|---|---|---|---|---|---|---|
| 1 | as-grown ZnTe crystal | | | | / | 183 | 2.2 | 14 |
| 2 | 5 | 40 | 11.1 | 50 | 1.1 | 181 | 2.3 | 6 |
| 3 | 5 | 40 | 11.1 | 100 | 1.2 | 184 | 2.0 | 10 |
| 4 | 5 | 40 | 11.1 | 200 | 1.4 | 186 | 1.8 | 15 |
| 5 | 0 | 45 | 0 | 200 | 1.4 | 185 | 2.0 | 14 |
| 6 | 5 | 40 | 11.1 | 300 | 1.5 | 187 | 1.7 | 16 |

# 3. Results and discussion

## 3.1. FIR reflection results

Assuming that the lattice vibration is the classical oscillator collection of transverse-optical (TO) phonons with a resonant frequency of $\omega_{TO}$, we can calculate the theoretical FIR reflection spectra with a standard optical multi-layer technique, where the surface damaged layer and the undamaged ZnTe crystal can be considered as the thin film layer and the substrate, respectively. Here we only consider the reflection from the vacuum-surface damage layer and the surface damaged layer-substrate interfaces, and the reflection coefficient $R$ can be obtained as[15]

$$R = \left| \frac{r_{vd} + a r_{ds}}{1 + a r_{vd} r_{ds}} \right|^2, \tag{1}$$

where $r_{vd}$ is the reflection coefficient from the vacuum to the surface damaged layer, $r_{ds}$ is the reflection coefficient from the surface damaged layer to the substrate and $a$ represents the phase difference and damping amplitude between two consecutive reflections in the surface damaged layer. In the normal incident case, $r_{vd}$, $r_{ds}$ and $a$ can be expressed as

$$r_{vd} = \frac{1 - n_d}{1 + n_d}, \quad r_{ds} = \frac{n_d - n_s}{n_d + n_s}, \tag{2a}$$

$$a = \exp\left( i \frac{2\omega d n_d}{c} \right), \tag{2b}$$

where $d$ is the average thickness of the surface damaged layer, $\omega$ is the FIR radiation frequency, $c$ is the velocity of light in vacuum and the complex indices ($n_d$ for the surface damage layer and $n_s$ for the substrate) are associated with the dielectric function by

$$n_{d,s} = \sqrt{\varepsilon_{d,s}}. \tag{2c}$$

The dielectric functions $\varepsilon_i(\omega)$ are modelled using a classical dielectric function for damped harmonic oscillators in combination with a Drude model:

$$\varepsilon_i(\omega) = \varepsilon_\infty + \frac{S_i \omega_{TO,i}^2}{\omega_{TO,i}^2 - \omega^2 - i\omega\gamma_i} - \frac{\varepsilon_\infty \omega_{p,i}^2}{\omega^2 + i\omega\gamma_{p,i}}, \tag{3}$$

where $\omega_{TO,i}$, $S_i$ and $\gamma_i$ are the frequency, oscillator strength and damping parameter of the TO phonon in the $i$th layer, respectively. $i$=d,s represent the surface damaged layer and the substrate, respectively. The first term $\varepsilon_\infty$ on the right-hand side of Eq.(3) is the high-frequency dielectric constant of the material. The second term is the lattice vibration contribution of the TO phonon. The third term describes the contribution of free carriers with plasma frequency $\omega_p$ and damping constant $\gamma_p$, which are given by

$$\omega_p^2 = \frac{4\pi n e^2}{\varepsilon_\infty m^*}, \tag{4a}$$

$$\gamma_p = \frac{e}{m^* \mu}, \tag{4b}$$

with $n$ being the free carrier concentration, $e$ the electron charge, $m^*$ the effective mass of carriers and $\mu$ the carrier mobility. As our p-type ZnTe has a carrier concentration of $10^{16}$–$3\times10^{17}\,cm^{-3}$, the third term has a much less contribution to $\varepsilon_i(\omega)$ which can be neglected compared with the first and second terms. Further considering the energy loss on the surface with a loss factor $L$, we have the reflection coefficient as follows

$$R = \left| r_{vd}(1 - L) + \frac{(1 - L)^2 (1 - r_{vd}^2) a r_{ds}}{1 + a r_{ds} r_{vd} (1 - L)} \right|^2. \tag{5}$$

By the aid of Eqs.(2), (3) and (5), and using $\varepsilon_\infty$=7.3,[18] $m^* = 0.6 m_0$ ($m_0$ is the electron mass), we can fit the FIR reflection spectra of all samples by adjusting the values of $\omega_{TO,i}$, $S_i$, $\gamma_i$ and $d$. Using a single-layer model ($n_d = n_s$), we first fit the FIR reflection spectrum of the as-grown ZnTe sample (No.1). These oscillator parameters were then incorporated as fixed parameters for the undamaged ZnTe crystals in the five RIE ZnTe samples. Figure 2 shows both the experimental (filled squares) and theoretical

(solid curves) results of the six ZnTe samples. They agree well with each other. Table 1 lists the detailed parameters of the multiple oscillators used for the fitting of measured reflection spectra of the five RIE ZnTe samples. It can be seen from the table that the oscillator strength $S$, the damping parameter $\gamma$ and the thickness $d$ change regularly with the, etching conditions. The variation of $\omega_{\mathrm{TO}}$ is within the measurement resolution and the fitting uncertainty. By analysing the four samples (Nos.2, 3, 4 and 6) etched under different rf plasma powers, we found that the oscillator strength $S$ decreases with increasing the rf plasma power, which basically satisfies the Lyddane–Sachs–Teller (LST) relation with $\omega_{\mathrm{TO},i}$:

$$S = \varepsilon_0 - \varepsilon_\infty \approx \varepsilon_\infty \left[ \left( \frac{\omega_{\mathrm{LO}}}{\omega_{\mathrm{TO}}} \right)^2 - 1 \right], \qquad (6)$$

where $\varepsilon_0$ is the static dielectric constant, and the LO frequency $\omega_{\mathrm{LO}}$=205.6cm$^{-1}$ is obtained from the Raman scattering results discussed in section 3.2. The damping parameter $\gamma$ increases with the rf plasma power, which represents the peak broadening in the FIR reflection spectra.

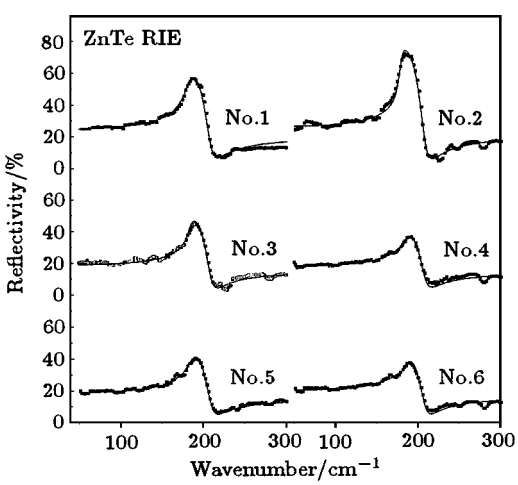



**Fig.2.** Experimental (filled squares) and theoretical (solid curves) FIR reflection spectra of the as-grown (No.1) and RIE ZnTe (Nos.2–6) crystals.

The most important result for us is the relationship between the average thickness of the surface damaged layer and the rf plasma power. From Table 1, the average thickness of the surface damaged layer is in the range of 1.1–1.5$\mu$m, which matches well with the scanning electron microscopy (SEM) results of 1.0–2.0$\mu$m. Furthermore, the average thickness of the surface damaged layer $d$ is found to increase with the rf plasma power. As we know, RIE is a mixed effect of the physical bombardment of ions and the chemical reaction of active particles, in which the ion bombardment is different from the physical process of sputtering, etching because it can enhance the chemical reaction. There are two mechanisms by which defects are induced in the surface damaged layers from dry processing. One is via a physical or sputtering mechanism from direct ion bombardment at the surface. If these defects had not diffused, they would only affect surface properties. They are removed continuously by, etching, except those at, etch-stop layers. The second mechanism for defect creation in crystalline materials is channelling, i.e. the propagation of ions along low-index directions of the lattice. Ions impinge upon the ample surface and most will be stopped rapidly by nuclear collisions. The dissipated energy will make the surface region disorder and cause some shallow channels, which will be deepened by the later-scattered ions. The defects induced owing to the two mechanisms will diffuse in the, etching process.[19,20] When the rf plasma power is increased, the energy of the electrons and incident ions is also increased, resulting in a stronger physical bombardment to the surface. At the same time, the intensity of active particles and ions is also increased, which makes the reaction of plasma more drastic. As a result, the defects induced by the two mechanisms are increased, leading to increasing the average thickness of the surface damaged layer.

Rahman *et al*[19,20] have studied in detail the above-mentioned two kinds of defects, especially the generation and diffusion of the second kind of defects. They have deduced the relationship between the defect density $n_{\mathrm{D}}$ and the depth $y$ below the surface

$$n_{\mathrm{D}}(y) = \frac{g_0}{\gamma'} \mathrm{e}^{-y/\lambda} + \frac{1}{v} \left( F - \frac{g_0 D}{\lambda \gamma'} \right) \mathrm{e}^{-yv/D}$$

$$(\tau > v^2/4D, D \geq \lambda v), \qquad (7a)$$

$$\gamma' = (v/\lambda)(1 - D/\lambda v), \qquad (7b)$$

$$n_{\mathrm{D}}(y) = \frac{\lambda g_0}{v} (1 - \mathrm{e}^{-v\tau/\lambda}) \mathrm{e}^{-y/\lambda}$$

$$(D \ll \lambda v, F = 0), \qquad (8)$$

where $v$ is the, etching rate, $\tau$ is the, etching time, $\lambda$ is the characteristic length of the channelling, $D$ is the diffusion coefficient of the defects, $F$ and $g_0 \mathrm{e}^{-y/\lambda}$ are the generation rates of the defects induced by the first and second mechanisms, respectively. Equations (7) and (8) describes the relationship of $n_{\mathrm{D}}$ and $y$ with and without considering the defect diffusion, respectively, from which we can find that $n_{\mathrm{D}}$ decreases as an exponent function with increasing $y$.

Take ZnTe sample No.2 as an example, by assuming $\lambda$=0.5$\mu$m, $g_0$=$10^{17}$cm$^{-3}$s$^{-1}$, $v$=15nm/min (estimated from Ref.[2]), $\tau$=10min and $D = F = 0$, according to Eq.(8), we obtain the defect density $n_D$~5.744×$10^{18}$cm$^{-3}$ at $y$=1.1$\mu$m. Our result is much larger than that of the RIE GaAs ($10^{17}$cm$^{-3}$) estimated by Rahman *et al*,[19] revealing that the RIE induced damage in ZnTe crystals is remarkable.

### 3.2.Raman scattering results

In order to reveal the effect of RIE processes on the surface of ZnTe crystals, we first carried out polarized Raman scattering measurements. It is expected that the damaged surface of, etched crystals will break the selection rules, which has been fully demonstrated in our experiments. Figure 3 shows the polarized Raman scattering spectra of the as-grown (No.1) and, etched ZnTe crystals (Nos.3 and 4) under the configurations of $z(x,x)\overline{z}$ (0° polarization) and $z(x,y)\overline{z}$ (90° polarization). The first-order LO phonons can be observed in all the three samples under the $z(x,x)\overline{z}$ configuration. However, under the $z(x,y)\overline{z}$ configuration, the LO phonon scattering is forbidden and we cannot observe it in the as-grown ZnTe crystal (No.1). The observation of the LO phonons in, etched ZnTe crystals (Nos.3 and 4), though they are much weak, clearly reveals the relaxation of the selection rules. The breaking of the selection rules can be attributed to the surface roughness of the, etched crystals, which clearly shows that the dry, etching has produced some damage in the surface of ZnTe crystals.

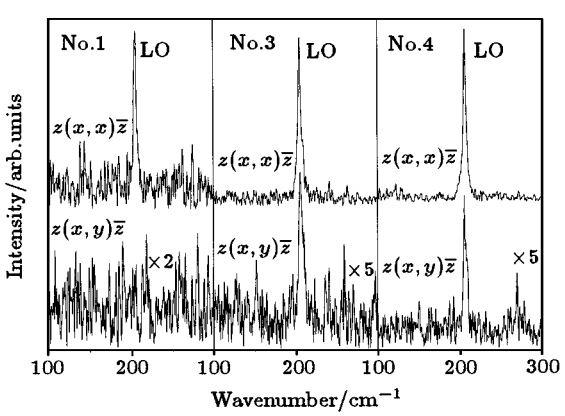



**Fig.3.** Polarized Raman scattering spectra of the as-grown (No.1) and, etched ZnTe (Nos.3 and 4) crystals under $z(x,x)\overline{z}$ (0° polarization) and $z(x,y)\overline{z}$ (90° polarization) configurations.

Wang *et al*[16] and Roughani *et al*[17] have studied the RIE damage in n$^+$-GaAs using the Raman scattering technique. They compared the intensity ratios of the LPP mode to the LO phonon mode ($I_{LPP}/I_{LO}$) for n$^+$-GaAs before and after, etching, and concluded that $I_{LPP}/I_{LO}$ decreases with increasing the dry, etching damage. This is in agreement with the reported result that the defects induced by RIE will decrease the carrier density and mobility.[19] In our Raman spectra of these RIE ZnTe crystals, the observed LO phonon at $\omega$=205.6cm$^{-1}$ is close to the reported one of 208.3±0.5cm$^{-1}$.[18] The TO phonons have also been observed due to the disorder-induced selection rule relaxation by the, etching. However, we will not discuss them in detail since they are much weaker compared with those of the second-order Raman scattering modes. The LPP mode was not observed due to the low carrier density in these p-ZnTe crystals; nevertheless, we can distinguish clearly the second-order Raman scattering modes. Figure 4 shows the normalized Raman scattering spectra of the five RIE ZnTe crystals to the first-order LO phonon of the as-grown ZnTe sample (No.1). The frequency variation of the second-order Raman modes is within ±2cm$^{-1}$ in these six ZnTe crystals. Table 2 lists the average frequencies of these second-order Raman modes, together with the reported frequencies, the calculated results from the second-neighbour ionic (SNI) model,[18] and the intensity ratios of the second-order Raman modes to the LO phonon ($I_{SO}/I_{LO}$). These results further verify the high quality of our ZnTe crystals and reveal the fact that RIE has little effect on the second-order Raman mode frequencies in ZnTe. From the data of sample Nos.1–4 and No.6 shown in the table, we find that the intensity ratio $I_{SO}/I_{LO}$ of every mode increases with the rf plasma power.

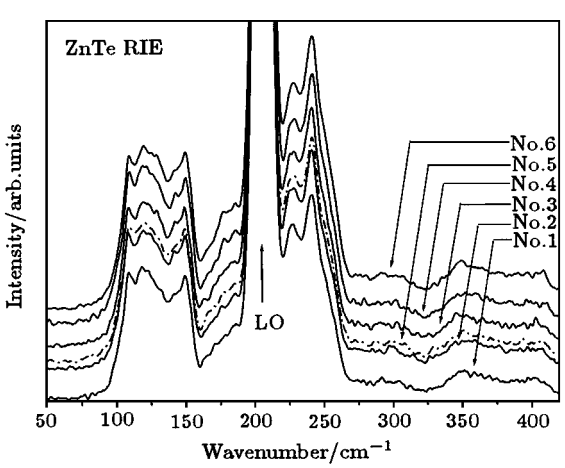



**Fig.4.** Raman scattering spectra of the as-grown (No.1) and RIE ZnTe (Nos.2–6) crystals. The intensity have been normalized to the first-order LO phonons of the sample No.1.

**Table 2.** Average frequency shifts and the intensity ratios of the second-order Raman modes to the LO phonon $I_{SO}/I_{LO}$, together with the reported frequency shifts and the calculated results from the second-neighbour ionic (SNI) model in Ref.[18].

| Assignment | Frequency shift/cm$^{-1}$ | | | $(I_{SO}/I_{LO})$/% | | | | | |
|---|---|---|---|---|---|---|---|---|---|
| | Our results | Reported data[18] | Calculated from SNI | No.1 | No.2 | No.3 | No.4 | No.5 | No.6 |
| 2TA($X$) | 108.9 | 108 | 108 | 3.68 | 3.95 | 4.01 | 4.37 | 3.92 | 4.39 |
| $2W_1$ | 119.6 | 116 | 114 | 3.85 | 4.00 | 4.16 | 4.52 | 4.00 | 4.74 |
| $W_1+W_2$ | 149.3 | 156 | 160 | 3.59 | 3.85 | 4.03 | 4.17 | 3.84 | 4.47 |
| TO($X$)+TA($X$) | 227.5 | 228 | 227 | 5.05 | 5.22 | 5.61 | 5.85 | 5.32 | 6.52 |
| LO($X$)+TA($X$) | 241.5 | 240 | 236 | 5.89 | 6.31 | 6.89 | 7.16 | 6.50 | 7.83 |
| 2LA($L$) | 282.5 | 282 | 286 | 0.54 | 0.63 | 0.68 | 0.77 | 0.63 | 0.98 |
| $2W_4, W_3+W_4$ | 290.8 | 290 | 292 | 0.66 | 0.59 | 0.72 | 0.66 | 0.54 | 1.06 |
| 2LA($L$) | 301.3 | 300 | 306 | 0.56 | 0.71 | 0.74 | 0.71 | 0.64 | 0.98 |
| TO($X$)+LA($X$) | 312.0 | 310 | 315 | 0.41 | 0.45 | 0.61 | 0.48 | 0.40 | 0.78 |
| [LO($L$)/TO($L$)]+LA($L$) | 327.5 | 329 | 326 | 0.34 | 0.39 | 0.40 | 0.35 | 0.46 | 0.76 |
| 2TO($X$), 2TO($L$) | 345.1 | 340 | 342 | 0.70 | 0.82 | 0.99 | 0.88 | 0.76 | |
| LO($X$)+TO($X$) | 351.8 | 349 | 355 | 0.85 | 0.85 | 0.93 | 0.92 | 0.93 | 1.41 |
| 2TO($\Gamma$) | 357.7 | 358 | 356 | 0.80 | 0.85 | 0.86 | 0.91 | 0.77 | 1.25 |
| 2LO($X$) | 364.4 | 364 | 364 | 0.75 | 0.77 | 0.84 | 0.81 | 0.85 | 1.19 |
| 2LO($\Gamma$) | 409.5 | 412 | 416 | 0.52 | 0.31 | 0.60 | 1.26 | 0.61 | 1.12 |
| LO | 205.6 | 208.3±0.5 | | | | | | | |

The second-order Raman scattering processes discussed here are mainly the two-phonon processes. This kind of two-phonon processes, depending on the energy of the two phonons, can be either the creation of two phonons with a Stokes component in the scattering spectra, or the creation of one phonon and the annihilation of the other. The probability of observing the second-order Raman modes in unetched samples can be described as[21]

$$P_\Sigma \propto 1+\frac{1}{\exp(h\nu_1/kT)-1}+\frac{1}{\exp(h\nu_2/kT)-1}$$

(creation of two phonons), (9)

$$P_\Delta \propto \frac{1}{\exp(h\nu_2/kT)-1}-\frac{1}{\exp(h\nu_1/kT)-1}$$

(creation of one phonon and annihilation of the other), (10)

with $\nu_1 > \nu_2$ being the phonon frequencies, $h$ the Planck constant, $k$ the Boltzmann constant and $T$ the temperature. From Eqs.(9) and (10), the intensities of the corresponding second-order Raman modes in these six ZnTe samples should be the same if they were all unetched. From the above FIR reflection results for the, etched ZnTe crystals (Nos.2–6), we understand that more defects and damage have been introduced into the crystals with increasing the rf plasma power, resulting in increasing the disorder in the crystals. It has been reported in Ref.[22] that $I_{SO}/I_{LO}$ increases with $x$ in $Mg_xZn_{1-x}Te$ crystals, due to the enhancement of the structural disorder in them. Although the induced disorder by RIE comes with a different mechanism from the $Mg_xZn_{1-x}Te$ crystals, we can demonstrate experimentally that the defect-induced disorder will also give an increase of $I_{SO}/I_{LO}$. Figure 5 shows the relationship between the $I_{SO}/I_{LO}$ and the rf plasma power $P$ for several strong second-order Raman modes, displaying the linear relationship between the $I_{SO}/I_{LO}$ and the rf plasma power (the points of $P$=0 represent the data of the as-grown ZnTe crystal). Combining with the FIR reflection results, we can have the following conclusion: with increasing rf plasma power, more defects and damage will be introduced in the crystals, and the thickness of the surface damaged layer will be increased and the disorder in the crystals will be enhanced; as a result, the intensity ratios of the second-order Raman modes to the first-order LO phonon will be increased accordingly, which have a linear relationship with the rf plasma power.

Finally, we analyse the effect of different $CH_4/H_2$ concentrations on the, etching through samples No.4 ($5CH_4/40H_2$) and No.5 ($0CH_4/45H_2$). The reported PL[23] and atomic force microscopy (AFM)[2] results have demonstrated that it is the physical ion bombardment, when the samples are, etched purely by $H_2$, that produces a strong damage in the crystal surface. With increasing $CH_4$ concentration, the chemical

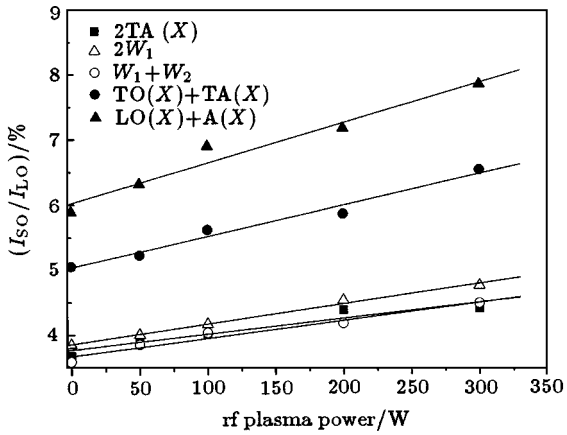



**Fig.5.** Relationship between $I_{SO}/I_{LO}$ (the intensity ratio of the second-order Raman modes to the LO phonon) and the rf plasma power $P$. $P$=0 represents the as-grown ZnTe crystal (No.1).

reaction is enhanced while the physical ion bombardment is weakened, leading to the weak damage in the surface. The strong surface damage in sample No.5 results in the small value of $I_{SO}/I_{LO}$ as compared with that in sample No.4. Nevertheless, the defect density in these two ZnTe crystals (Nos.4 and 5) is on the same order; therefore, there is not much difference in their FIR reflection spectra shown in Fig.2.

## 4. Conclusions

By studying the FIR reflection spectra of dry, etching p-ZnTe crystals under different conditions, we have obtained the average thickness of the surface damaged layer being in the range of 1.0–1.5$\mu$m, and the estimated defect intensity in the order of $10^{18}$cm$^{-3}$. The results demonstrate that the defects induced by the electrons and incident ions increase with the rf plasma power. The polarized Raman scattering measurements have revealed the RIE-induced surface damage in ZnTe crystals. The relationship between the intensity ratio $I_{SO}/I_{LO}$ and the rf plasma power has been obtained from the Raman scattering results for different RIE ZnTe samples. Our conclusions can be stated as: more defects and damage will be introduced in the crystals with increasing rf plasma powers, the thickness of the surface damaged layer will be increased and the disorder in the crystals will be enhanced accordingly, resulting in a linear relationship between the rf plasma power and the intensity ratio $I_{SO}/I_{LO}$.

## References


[1] Chai C C, Yang Y T, Li Y J, Jia H J and Ji H L 1999 *Acta Phys. Sin.* **48** 550 (in Chinese)
Zhang J, Feng R B, Du C L, Wang Y R, Zhou L S, Hou D S and Lin D J 1997 *Optoelectron. Eng.* **24** S46 (in Chinese)

[2] Guo Q X, Matsuse M, Tanaka T, Nishio M, Ogawa H, Chang Y, Wang J and Wang S L 2001 *J. Vac. Sci. Technol.* A **19** 2232

[3] Murad S, Rahman M, Johnson N, Thoms S, Beaumont S P and Wilkinson C D W 1996 *J. Vac. Sci. Technol.* B **14** 3658

[4] Cheung R, Lee H Y, Lee K Y, Smith III T P, Kern D P, Beaumont S P and Wilkinson C D W 1989 *J. Vac. Sci. Technol.* B **7** 1462

[5] Ermolieff A, Amouroux A, Marthon S, Daviet J F and Peccoud L 1991 *Semicond. Sci. Technol.* **6** 290

[6] Cheung R, Thoms S, Beaumont S P, Doughty G, Law V and Wilkinson C D W 1987 *Electron. Lett.* **23** 857

[7] Wilkinson C D W 1990 *Superlatt. Microstruct.* **7** 381

[8] Germann R, Forchel A, Bresch M and Meier H P 1989 *J. Vac. Sci. Technol.* B **7** 1475

[9] Watt M, Sotomayor-Torres C M, Cheung R, Wilkinson C D W, Arnot H E G and Beaumont S P 1988 *J. Mod. Opt.* **35** 365

[10] Taike A, Momose M, Kawata M, Gotoh J and Mochizuki K 1996 *J. Cryst. Growth* **159** 714

[11] Sato K, Asahi T, Hanafusa M, Noda A, Arakawa A, Uchida M, Oda O, Yamada Y and Taguchi T 2000 *Phys. Status Sol.* A **180** 26

[12] Bhunia S and Bose D N 2000 *J. Appl. Phys.* **87** 2931

[13] Chen W R, Chang S J, Su Y K, Lan W H, Lin A C H and Chang H 2000 *Japan. J. Appl. Phys.* **39** 3308

[14] Yu G, Jiang L F, Shen W Z and Wu H Z 2002 *J. Phys. D: Appl. Phys.* **35** 57

[15] Qian Z G, Yu G, Shen W Z, Ogawa H and Guo Q X 2002 *Physica* B **318** 180

[16] Wang P D, Foad M A, Sotomayor-Torres C M, Watt M, Cheung R, Wilkison C D W and Beaumont S P 1992 *J. Appl. Phys.* **71** 3754

[17] Roughani B, Jackson H E, Jbara J J, Mantei T D, Hickman G, Stutz C E, Evans K R and Jones R L 1989 *IEEE J. Quantum Electron.* **25** 1003

[18] Irwin J C and LaCombe J 1969 *J. Appl. Phys.* **41** 1444

[19] Rahman M 1997 *J. Appl. Phys.* **82** 2215

[20] Rahman M, Deng L G, Wilkinson C D W and van den Berg J A 2001 *J. Appl. Phys.* **89** 2096

[21] Schall M *et al* 2001 *Phys. Rev.* B **64** 94301

[22] Yoon C S, Kim B H, Cha D, Kim Y S, Chung S J, Ko J G, Kim C D, Park H L and Kim W T 1998 *Solid State Commun.* **106** 481

[23] Guo Q X, Matsumoto Y C, Wang S L, Tanaka T, Nishio M and Ogawa H 2002 *Japan. J. Appl. Phys.* **41** 5069